(4)

Annual Letter Report

Pseudomorphic Semiconducting Heterostructures from Combinations of AlN, GaN and Selected SiC Polytypes: Theoretical Advancement and its Coordination with Experimental Studies of Nucleation, Growth, Characterization and Device Development

Supported under Grant #N00014-90-J-1427
Department of the Navy
Office of the Chief of Naval Research
Report for the period January 1, 1990–December 31, 1990

Robert F. Davis, Max W. H. Braun, Larry Rowland,
Zlatko Sitar, and Andrej Skerlavaj
Materials Science and Engineering Department
North Carolina State University
Campus Box 7907
Raleigh, NC 27695-7907

December, 1990

REPORT DOCUMENTATION PAGE

Form Approved
OMB No 0704-0188

1. AGENCY USE ONLY (Leave blank)	2. REPORT DATE	3. REPORT TYPE AND DATES COVERED
	December, 1990	Annual Letter 1/1/90-12/31/90

4. TITLE AND SUBTITLE Pseudomorphic Semiconducting Hetero-structures from Combinations of AlN, GaN and Selected SiC Polytypes: Theoretical Advancement and its Coordination with Experimental Studies

5. FUNDING NUMBERS

414s007---01
1114SS
N00179
N66005
4B855

6. AUTHOR(S)

Robert F. Davis

7. PERFORMING ORGANIZATION NAME(S) AND ADDRESS(ES)

North Carolina State University
Hillsborough Street
Raleigh,NC 27695

8. PERFORMING ORGANIZATION REPORT NUMBER

N00014-90-J-1427

9. SPONSORING/MONITORING AGENCY NAME(S) AND ADDRESS(ES)

Department of the Navy
Office of the Chief of Naval Research
800 North Quincy, Code 1513:CMB
Arlington, VA 22217-5000

10. SPONSORING/MONITORING AGENCY REPORT NUMBER

11. SUPPLEMENTARY NOTES

12a. DISTRIBUTION/AVAILABILITY STATEMENT

Approved for Public Release; Distribution Unlimited

12b. DISTRIBUTION CODE

13. ABSTRACT (Maximum 200 words)

In this reporting period, research has been conducted in three primary areas: (1) development and application of computer codes concerned with the prediction of properties of pseudomorphic structures, (2) the growth of GaN/AlN pseudomorphic structures and (3) the construction of a growth system for the deposition of SiC/AlN/GaN pseudomorphic structures. The van der Merwe-Reiss rigid model has been extended theoretically via computer algorithms for polyatomic systems by allowing several interaction potentials to act simultaneously between overgrowth atoms and the substrate across planar interfaces. These adaptations have also been applied to an extended model which includes homogeneous strain and thickness. In this latter model, epitaxial orientations are predicted to be those which minimize strain and misfit energies together. Experimentally, AlN/GaN layered structures have been grown using a modified gas source MBE technique. Layers as thin as two monolayers have been grown. In addition, a second modified gas source MBE for the growth of SiC/AlN/GaN pseudomorphic layers is being constructed, it is described in detail.

14. SUBJECT TERMS	15. NUMBER OF PAGES
pseudomorphic heterostructures, gallium nitride, aluminum nitride, gas-source molecular beam epitaxy	44
	16. PRICE CODE

17. SECURITY CLASSIFICATION OF REPORT	18. SECURITY CLASSIFICATION OF THIS PAGE	19. SECURITY CLASSIFICATION OF ABSTRACT	20. LIMITATION OF ABSTRACT
UNCLAS	UNCLAS	UNCLAS	SAR

Table of Contents

I. Introduction

The advent of techniques for growing semiconductor multilayer structures with layer thicknesses approaching atomic dimensions has provided new systems for both basic physics studies and device applications. Most of the research involving these structures has been restricted to materials with lattice constants that are equal within $\simeq 0.1\%$ However it is now recognized that interesting and useful pseudomorphic structures can also be grown from a much larger set of materials that have lattice-constant mismatches in the percent range. Moreover, advances in computer hardware and software as well as the development of theoretical structural and molecular models applicable for strained layer nucleation, growth and property prediction have occurred to the extent that the field is poised to expand rapidly. It is in this context that the research described in this report is being conducted. The materials systems of concern include combinations of the direct bandgap materials of AlN and GaN and selected, indirect bandgap SiC polytypes.

The extremes in thermal, mechanical, chemical and electronic properties of SiC allow the types and numbers of current and conceivable applications of this material to be substantial. However, a principal driving force for the current resurgence in interest in this material, as well as AlN and GaN, is their potential as hosts for high power, high temperature microelectronic and optoelectronic devices for use in extreme environments. The availability of thin film heterostructural combinations of these materials will substantially broaden the applications potential for these materials. The pseudomorphic structures produced from these materials will be unique because of their chemistry, their wide bandgaps, the availability of indirect/direct bandgap combinations, their occurrence in cubic and hexagonal forms and the ability to tailor the lattice parameters and therefore the amount of strain and the physical properties via solid solutions composed of the three components.

In this reporting period, the P.I. and his coworkers have conducted studies in three primary areas of the grant: (1) development and application of computer codes concerned with pseudomorphic structures and which specifically address the prediction of epitaxial configurations in covalent systems (M. W. H. Braun); (2) the growth of GaN/AlN pseudomorphic heterostructures (Z. Sitar); (3) the atomic layer epitaxy of GaN and AlN (Z. Sitar and A. Skerlavaj) and (4) the design and fabrication of a growth system for the deposition SiC/AlN/GaN pseudomorphic structures (L. Rowland). The procedures, results and a discussion of these results and directions for future research are presented in the following sections.

II. Computer Codes for Prediction of Epitaxial Configurations of Polyatomic Covalent Systems

A. Introduction

The previous report (July, 1990) for this grant documented the details of our theoretical study of the pseudomorphic system diamond-cubic boron nitride (cBN). This materials system was selected because of its current importance to U. S. technology and because it was an excellent model system which could be used for developing and evaluating the new computer codes for pseudomorphic systems developed under this grant. Specifically, the report described the principles of interfacial considerations in pseudomorphic systems in terms of the Van der Merwe-Reiss rigid model [1-3] which follows a derivation given by Braun of an epitaxial criterion formulated in reciprocal space. The reciprocal space and direct space consequences of the criterion were also reviewed. These considerations were then applied to the matching conditions of the low index like faces of diamond and cBN as well as the mixed face pairs of diamond {100}, {110}, {111}, {112}, {114} and {120} on cBN {221} and diamond {110} on the cBN{120} face, diamond {100} on cBN{110}, and diamond {100}, {110} and {111} on the cBN{112} face. Some unique aspects of the diamond {100}, cBN{221} pair were highlighted. To

save space only a brief summary on this research will be presented in this Annual Letter Report.

The results showed that the two-dimensional pseudomorphic matching between diamond and cBN is only a little more costly in strain energy than one-dimensional pseudomorphy in like planes. The second best matching possibility is the diamond{100} on cBN{221} case, identical in strain energy to pseudomorphic cases, but with increased misfit energy. The realization of either or both of {100} or {221} with the {221} substrate will clearly depend on growth conditions. Of other unlike pairs, the diamond{100} on the cBN{112} configuration has a two dimensional configuration with a strain energy density of 1.35×10^9erg cm^{-3} and comparable to the one dimensional case. However, this is only a rather high order coincidence match in which every fifth substrate reciprocal lattice point coincides with every second overgrowth point resulting in a high misfit energy. It is better than one dimensional matching, but somewhat unfavorable when compared to the possibility of pseudomorphic diamond{112} on cBN{112}. Other unlike planes do not have the possibility of two dimensional coherency within such a low energy thus making it unlikely that unlike planes will grow epitaxially.

Therefore it may be concluded that the diamond-cBN system appears to agree with the geometric considerations as expressed in the reciprocal lattice criterion. Moreover, low index like planes have been observed to grow pseudomorphically experimentally, and the geometrically derived low required strain of 1.37% from bulk parameters is consistent. The unlike epitaxial configuration which pairs diamond{100} with cBN{221} yields two-dimensional coincidence with the same small strain, and is favoured above other low-index mixed configurations in this way. The reason for observed {100} growth as opposed to {221} growth of the diamond is probably due to surface energy properties and conditions during growth, although as was pointed out, the experiment itself is ambiguous

about the possibility that the {221} orientation is actually retained in the interface, transforming into a {100} orientation some distance away from the interface.

The rigidity of diamond suggests that geometric criteria are particularly suitable as a tool for selecting candidate substrate planes, particularly important where structures of dissimilar types are considered as substrate candidates. The reciprocal lattice provides clarity where considerations with atomic rows tend to be clouded by details of atomic positions.

In this report we describe computer codes applicable to the problem of epitaxy in covalent overgrowth-substrate systems and the theories on which they are based.

The general condition for the formation of a monolayer may be formulated as an inequality requiring a free energy reduction [4,5], as

$$\gamma_O - \gamma_S + \gamma_I \leq 0 \qquad (1)$$

where γ_O and γ_S are the surface free energy of the overgrowth and substrate respectively, and γ_I is the energy associated with the formation of the interface. In the presence of misfit the last term contains the competing *elastic strain energy* in the monolayer and *misfit energy* of interfacial disregistry. These depend on the interface geometry, the strength and details of the overgrowth-substrate interaction and the elastic properties of the materials forming the bicrystal.

The theory and computer codes described here address the interfacial energy term on two levels of sophistication. First the conditions under which given crystal structures minimize the interfacial energy without deformation are considered. These epitaxial configurations are termed the ideal epitaxial configurations by van der Merwe. [1] The van der Merwe-Reiss rigid model has been adapted for covalent systems by taking account of the different interactions which overgrowth atoms experience with the substrate, depending on the number and directions of adatom-substrate bonds. Similarly, these extensions have also been applied to the next level, in which the overgrowth is

allowed to strain to achieve pseudomorphism. This theory predicts epitaxial orientations and the existence or absence of pseudomorphism by determining the conditions of orientation and homogeneous strain which minimizes the sum of the misfit and strain contributions to the interfacial energy [1,3,6].

The computer codes ELCON, MULTIMIS and PSEUDO are completely rewritten and generalized versions of an earlier suite of specialized programs serving a similar purpose for somewhat simpler metal systems. We describe their functions and present some sample output of the program MULTIMIS.

B. Models of Epitaxy in Covalent Systems

1. The Rigid Model

The Basic Model. In the geometric limit both components of the bicrystal are considered rigid, retain their bulk lattice structures and parameters and are in contact at a single interfacial plane. On either side of the interface each component crystal presents a crystal plane with unique translational and rotational symmetries. The periodicities are described by infinite sets of wave vectors which form the surface reciprocal lattices for each crystal face.

The interaction energy between an individual interfacial overgrowth atom (adatom) and the substrate surface is assumed to be dependent on position and to have the symmetry of the substrate surface. The energy is therefore given in Fourier form as the potential

$$V(x,y) = W \sum_{\{\mathbf{q}\}} V_{\mathbf{q}} \exp(i\mathbf{q}\cdot\mathbf{r}) = W \sum_{h,\,k=-\infty}^{\infty} V_{hk} \exp[i2\pi\,(hx+ky)] \qquad (2)$$

where $\mathbf{q} = h\mathbf{a}_1^* + k\mathbf{a}_2^* \equiv \mathbf{q}_{hk}$ is a lattice translation vector of the substrate surface reciprocal lattice (defined by the condition $\mathbf{a}_i \cdot \mathbf{a}_j^* = 2\pi\delta_{ij}$, i,j = 1,2) and h and k are required to be integers. In this expression, $V_{\mathbf{q}}$ and V_{hk} are Fourier coefficients appropriate to the two equivalent forms of the series, and W is an overall scale factor

which allows the Fourier expansion itself to be expressed in a normalized form. Position in the substrate surface lattice is given by $\mathbf{r} = x\mathbf{a}_1 + y\mathbf{a}_2$, where $\mathbf{a}_1$ and $\mathbf{a}_2$ are basis vectors of the substrate surface unit cell.

The basic model [1,3] assumes that all interfacial overgrowth atoms experience the same potential. The overgrowth-substrate interaction is then the sum of the individual values for each of the atoms, depending only on their positions in the substrate unit cell. An overgrowth island is constructed to contain $(2M+1)\times(2N+1)$ overgrowth lattice points. These are arranged as $2N+1$ rows of $2M+1$ points each, and are obtained by displacing a single (central) point by all the vectors in the set

$$\{\mathbf{r}_b = m\mathbf{b}_1 + n\mathbf{b}_2 : m = -M, \ldots 0, \ldots M;\ n=-N, \ldots 0, \ldots N\} \qquad (3)$$

where $\mathbf{b}_1$ and $\mathbf{b}_2$ are basis vectors of the overgrowth surface unit cell. The limit as $M,N \rightarrow \infty$ describes a monolayer. In general, the most convenient choice of overgrowth and substrate origins may not coincide, and the displacement $\mathbf{r}_o = x_o\mathbf{a}_1 + y_o\mathbf{a}_2$ is introduced.

It is assumed that the origin of the overgrowth lattice is placed at a minimum of energy in the substrate potential, (eq. 2). The energy scale is chosen in such a way that if every overgrowth atom lies at an exact minimum of the substrate, the total energy given by expression (2) will be zero. Any deviation from this exact matching situation (*misfit* then exists) yields an energy greater than zero. With this choice the energy is interpreted directly as *misfit energy*. A quantitative model requires that the Fourier coefficients be known, and normally the series will be truncated after a few terms.

After summing individual energy contributions over all the atoms in the overgrowth island, the total interaction energy *per atom* for G overgrowth atoms is

$$V = \frac{W}{G} \sum_{h,k} V_{hk} F_o^{hk} \frac{\sin \pi(2M+1)p(h,k)}{\sin \pi p(h,k)} \cdot \frac{\sin \pi(2N+1)q(h,k)}{\sin \pi q(h,k)} \qquad (4)$$

where $F_o^{hk} = \exp[i2\pi(hx_o+ky_o)]$ is a structure factor due to the relative translations of the origin and the substrate.

The relationship between the pairs p, q and h, k is given by the expressions

$$p(h,k) = hr_{11}\, c_\theta + kr_{12}\, s_\theta \quad , \quad q(h,k) = hr_{21}\, s_{\theta\beta} + kr_{22}\, c_{\theta\beta} \qquad (5a)$$

with θ the angle between $\mathbf{b}_1$ and $\mathbf{a}_1$ and

$$r_{ij} = b_i/a_j = C_{bi}\, b_{nn}/C_{aj}\, a_{nn} = (C_{bi}/C_{aj})r \quad , \quad r = b_{nn}/a_{nn} \quad i,j = 1, 2 \qquad (5b)$$

$$c_\theta = \sin(\alpha-\theta)/\sin\alpha \quad , \quad s_\theta = \sin\theta/\sin\alpha \, ,$$

$$s_{\theta\beta} = \sin(\alpha-\beta-\theta)/\sin\alpha \quad , \quad c_{\theta\beta} = \sin(\beta+\theta)/\sin\alpha$$

while r is termed the ratio of nearest neighbor distances, a_{nn} and b_{nn}, or simply the nearest neighbor ratio. This identifies with the atomic size ratio introduced by Bruce *et al.* Other quantities are the substrate and overgrowth surface unit cell angles, α and β, and the lengths of the surface cell basis vectors, a_i and b_i.

Direct calculation of the transformation between the $\mathbf{b}_1, \mathbf{b}_2$ and $\mathbf{a}_1, \mathbf{a}_2$ systems shows that p(h,k) and q(h,k) are the overgrowth reciprocal lattice coordinates of the substrate wave vector $\mathbf{q}_{hk}$. The energy in eq. (3) peaks sharply when p and q are integers. When this necessary condition is met the misfit energy is sharply minimized when the product of the sine terms and the resonating V_{hk} is negative.

Generalization to Multiple Atom Types. The above model has been formulated for a monatomic overgrowth, with only a single non-directional bond type active between the overgrowth and the substrate, qualitatively, a good representation of metal systems. Several generalizations may be introduced [3], some useful in metal systems, but most essential in covalent systems.

If several atomic species (or several bond types) are in the interface, both the interaction potential and the overgrowth island must provide more features than the primitive lattice assumed in the basic model.

If the basic potential is simply repeated, but displaced in the unit cell, then the potential is modified by a simple structure factor, $\exp[-hx^{+}-ky^{+}]$. When generalized to several such additions, and an overall factor to represent attenuation, for example, the structure factors add to a single term

$$F_{hk}= \sum_{i} \Delta_i \exp[-hx_i^{+}-ky_i^{+}] \tag{6}$$

where the sum is taken over all such features of interest. This yields a generalized form for the interaction potential for a given overgrowth atom as

$$V(x,y) = W \sum_{h,\,k=-\infty}^{\infty} V_{hk}\, F_{hk}\, \exp[i2\pi\,(hx+ky)] \tag{7}$$

The advantage of the formulation is that the structure factor and its product with the coefficient can be pre-calculated for a given overgrowth atom type, and remains of essentially the same form as in the basic model, but contains considerably more structural information.

Additional atoms in the overgrowth introduce further structure factors which depend on the exact transformation between the overgrowth and substrate coordinate systems, i.e the orientation and state of strain, as they depend on the p(h,k) and q(h,k) terms. Additionally, these atoms may experience the substrate in the same way, or in attenuated form, or even so differently that entirely separate substrate potentials need to be introduced. In this general case the misfit energy per interfacial atom becomes

$$V = \frac{W}{G} \sum_{t} W_t \sum_{h,\,k} V_{hk}^{t}\, F_{hk}^{t}\, F_{o}^{hk}\, F_{t}^{pq}\, \frac{\sin \pi(2M+1)p(h,k)}{\sin \pi p(h,k)} \cdot \frac{\sin \pi(2N+1)q(h,k)}{\sin \pi q(h,k)} \tag{8}$$

where the outer summation is over the types of overgrowth atom which each require a different substrate potential, and G is the total number of interfacial atoms. Here, W is an overall scale factor, and the W_t are most useful as relative weight factors.

It is this very general form which is used in the computer codes we have written, but rather than using exponential forms for the potential and the structure factors, only cosine terms have been used. The compact form of eq 8 is lost to some extent as a result. While complicating the computer programs in one sense, the ease of use is enhanced, in that the potentials are easier to construct (only real, rather than complex, coefficients are needed), and are also more easily implemented on different computers, as not all useful computer languages support operations between complex numbers.

2. Homogeneous Strain and Pseudomorphism

When the overgrowth does not exactly fit the substrate to minimize or zero the misfit energy in some epitaxial orientation, it may be expected to deform at a cost of strain energy while it is energetically favorable. This means that the unit cell of the overgrowth is deformed so that some lattice spacing of the overgrowth nearly fits the substrate. Exact fits will only occur in infinite systems, and the computer code ORPHEUS, described elsewhere [3,7], calculates the strains for exact match in those cases. The program described below is applicable to both finite and infinite systems and calculates the strains by direct numerical minimization of the total energy [3,6].

Strain Energy. The strains are expressed in a Cartesian coordinate system based on the unit cell coordinates of the overgrowth, in which the x-axis of the Cartesian system is parallel to the $\mathbf{b}_1$ axis of the overgrowth unit cell. The z-axis is perpendicular to and points away from the interface plane. The elastic constants for any overgrowth material must be transformed to this coordinate system, and then reduced to two-dimensional form by applying plane stress boundary conditions which are applicable to structures which are large in extent in two dimensions, but relatively thin in the third dimension. The stress in the overgrowth is assumed to be independent of the z-component, and no stress

components act in the upper (free) surface. A computer program ELCON provides Voigt averaged isotropic constants, and the required two-dimensional elastic constant matrices for any crystal structure and any plane entered in crystallographic conventional notation, when given the appropriate elastic constants in standard (reduced) notation.

The general expression for the elastic energy per interfacial atom is given as

$$\xi = \frac{1}{2}\left[D_{11}\,\varepsilon_x^2+D_{22}\,\varepsilon_y^2+2D_{12}\,\varepsilon_x\,\varepsilon_y+2D_{13}\,\varepsilon_x\,\gamma_{xy}+2D_{23}\,\varepsilon_y\,\gamma_{xy}+D_{33}\,\gamma_{xy}^2\right]\Omega_b \qquad (9a)$$

where Ω_b is the volume of the overlayer, per interfacial atom. The expression simplifies in the case of an isotropic overgrowth, to the form

$$\xi = \frac{\mu}{(1-\nu)}\left[\varepsilon_x^2 + \varepsilon_y^2 + 2\nu\,\varepsilon_x\,\varepsilon_y + (1-\nu)\,\gamma_{xy}^2\right]\Omega_b \qquad (9b)$$

It is this second form which is used to characterize the pair of materials by rigidity, strength of the overgrowth/substrate bonding and the degree of misfit by the parameter introduced by van der Merwe [8,9],

$$\mathfrak{Q}^2 = \frac{\mu\Omega_b}{(1-\nu)\,W\,r^2} \qquad (10)$$

Although this parameter has been used in an anisotropic version (using D_{11} instead of $2\mu/(1-\nu)$ as elastic factor, it is more useful when comparing general behavior of materials (including non-cubic materials) to use the isotropic parameter as a basis for comparison. For this reason the generalized program PSEUDO requires that both the general plane stress elastic constant matrix (D_{ij}) and the Voigt averaged elastic constants, μ and ν are provided.

Effect of Strain on the Misfit Energy. The strain affects the misfit energy by directly changing overgrowth unit cell parameters.

Thus the overgrowth unit cell parameters become:

$$b_1' = b_1\sqrt{(1+\varepsilon_x)^2 + \gamma_{xy}^2}$$

$$b_2' = b_2\sqrt{\left[(1+\varepsilon_x)\cos\beta + \tfrac{1}{2}\gamma_{xy}\sin\beta\right]^2 + \left[\tfrac{1}{2}\gamma_{xy}\cos\beta + (1+\varepsilon_y)\sin\beta\right]^2}$$

$$\delta\phi_1 = \arctan\left[\tfrac{1}{2}\gamma_{xy}/(1+\varepsilon_x)\right]$$

$$\delta\phi_2 = \arctan\left[\left[(1+\varepsilon_x)\cos\beta + \tfrac{1}{2}\gamma_{xy}\sin\beta\right] / \left[\tfrac{1}{2}\gamma_{xy}\cos\beta + (1+\varepsilon_y)\sin\beta\right]\right]$$

so that

$$\theta' = \theta + \delta\phi_1$$

$$\beta' = \beta - (\delta\phi_1 + \delta\phi_2)$$

The correct misfit energy is then given by Eq. 8, but with the new lattice parameters.

C. The Computer Codes

Three main computer programs have been generalized and rewritten for this project.

1. ELCON

To transform elastic constants for any crystal class to the required Cartesian coordinate system in any crystal plane (specified in crystallographic convention), the program ELCON was generalized. This program transforms creates and transforms the elastic constant tensor to the required coordinate system, provides the reduced notation elastic constants and generates the two-dimensional plane stress elastic constant matrix. Additionally, the program provides Voigt averaged isotropic elastic constants and the plane stress matrix. These are necessary for the construction of phase diagrams which provide qualitative information about the behavior of structure types, concerning epitaxial configurations and whether superlattices can be created from them. The present implementation is written in the MICROSOFT QUICKBASIC dialect for the Apple Macintosh computer. All input is interactive, and the user is lead through the various input stages by questions and even checks whether inputs are reasonable.

2. MULTIMIS

This program implements the general form of the rigid model to create graphs of the misfit energy vs nearest neighbor ratio (r) and orientation θ. Additionally, structure factors and p,q values are produced so that the minimizing configurations can be specified in terms of crystallographic conventions and spacings. This latter interpretation is done with the program ORPHEUS, which has been ported to the Macintosh computer, in MICROSOFT QUICKBASIC, and generalized to provide general structure factor data and direct-space crystallographic information.

This program, and PSEUDO, below, use only the real portion of the Misfit Energy expression, by basing the adatom-substrate potential entirely on cosine (and displaced cosine) functions. No loss of generality is introduced in this way, the displacement of cosine functions introduces the effect of the sine functions in any case, and the reciprocal lattice itself always has inversion symmetry, making the (even) cosine functions natural.

MULTIMIS is written in FORTRAN 77, but depends on the CA-DISSPLA package [10] for graphics output. This package is available on the CRAY Y-MP computer at the North Carolina Supercomputer Center in the Research Triangle Park. A typical computer run takes a few seconds to produce a diagram based on 4000 data points.

3. PSEUDO

This most general computer program produces several types of output and is used to predict the configurations which particular crystal structures can reach by pseudomorphic strain. The overgrowth strains if the interfacial energy is reduced by straining compared to the unstrained case. Once again, once the strains are known, the Burgers' vectors and spacings of misfit dislocations can be determined directly from the program ORPHEUS.

The types of data produced by the PSEUDO program include minimized total interfacial energies and the separate misfit and elastic energies for a range of orientations

and nearest neighbor ratios, including the rigid, undeformed energies. The data are produced subject to several constraints, which each have their own usefulness to aid interpretation.

•Constant interfacial energy amplitude W : (or several values of W, in steps)

Rigid misfit energy, Minimized total energy, strain energy, strained misfit energy, strains, structure factors and p,q vs h,k component pairs. (When p and q are nearly integer the configuration corresponding to that pair of orientations has been achieved, and the properties of the configuration can be determined from reciprocal space considerations using the program ORPHEUS)

•Constant configuration parameter ℓ: (W derived by eq 10): (or several values of ℓ in steps)

The same output forms as in a)

• Phase information:

Subject to orientation angle θ, (ideally several individually specified orientations which have been determined by step a or b to be possible for particular structural types) the various energies are produced vs ℓ and r. It should be noted at this point that the parameter ℓ contains the volume of overgrowth material per interfacial atom, and therefore implicitly contains the thickness. By plotting the configurations (Pseudomorphic, 1-Dimensional, misfitting) which occur in regions of ℓ and r, a critical thickness for the particular combination of lattice parameter, interfacial bond strength and overgrowth rigidity can be determined for the breakdown of particular epitaxial configurations. This feature promises to be the most useful, once the program PHASE which extracts this information from the output produced by PSEUDO has been generalized and ported to the CRAY computer. (At present PHASE is still applicable only to specific cubic interfaces and not general systems)

Additionally, all the above data can be produced for a single r-θ pair, for a range of r and fixed θ, fixed r but a range of θ, and range of r and θ.

Some technical generalizations have been included in the code, including a feature to allow the construction of symmetrical islands, by allowing the structure of boundary unit cells to be specified separately from the general repeating unit cell forming the major part of the island. This is useful both as an internal test for the verification of the program (diagrams must be symmetrical if the overgrowth or substrate are symmetrical, and orientations aries from rotation about the symmetry axes), and to allow a significant range of orientation angle to serve for the entire 360 degree field.

The subroutine BCONF from the IMSL [11] package is used to determine the minima of the total energy. Starting values for misfits strains which are forced on the routine are 1) no strain, 2) strains which allow the overgrowth to match exactly with the substrate in specific epitaxial configurations determined for the structures from MULTIMIS or ORPHEUS, for both 1-Dimensional and 2-Dimensional pseudomorphic configurations. Additionally, the best value of a neighboring point's strains are also forced on the program. Finally, over thirty systematically spaced points in the three-dimensional $\{\varepsilon_x , \varepsilon_y , \gamma_{xy}\}$ - space bounded by ±30% in the three directions are used as initial values for minimization, which is allowed to proceed for a small number of steps (30) before being stopped. The best five minimizations of this latter series are then allowed to converge completely.

The reason for this multiply starting minimization is that the strain energy itself is smoothly paraboloid in behavior, while the misfit energy tends to be nearly flat plateau, with a spiked depression. (See fig. 2 for an example.) The danger exists that the behavior of the elastic energy will dominate over the flatter misfit energy in the gradient search methods, so that the global minimum is missed. The procedure above produces a correct global minimum with high reliability, particularly if the overgrowth islands are not chosen to be too large (M or N greater than 100). For large values of M, N the performance of the program improves if the strains are stepped in small increments, and the program compiled in double precision.

The standard version of the program at present produces a minimized set of data every 1.5 CPU seconds on the CRAY Y-MP, although this figure should improve with development, as the starting values are chosen on a better range.

D. Results and Discussion

We present some sample outputs from the program MULTIMIS and a short discussion of the verification process of the program PSEUDO.

The diagrams of Fig. 1 are typical of the type of output produced by MULTIMIS. In the present version of the program the headings and axis titles are generic, although a future version will give a user full control over these aspects, and the annotation information. In addition to misfit energies, the program provides plots of the adatom-substrate interaction potential, (Fig. 1) which allows one to directly visualize and confirm that the potential has the physical features desired of the model. These and the misfit energies are available as contour diagrams, perspective wire-mesh 3D diagrams and as sectional 2-dimensional line curves. The misfit energy diagram in Fig. 2, for example shows a large range of lattice parameter ratios, and the sharp depressions which occur in the misfit energy at Ideal Epitaxial configurations. The sectional diagram of Fig. 3 shows the misfit energy for a particular lattice parameter ratio, r= 0.986 , and the orientations which produce minima.

As described in the discussion of the program capabilities, the program PSEUDO has not been fully tested. However, the rigid overgrowth values of this program and MULTIMIS do agree. Another test is whether the strains predicted for the configurations close to Ideal epitaxial configurations must yield matching with that configuration, particularly for high coupling strengths, W. This test has been carried out at single sample points. The overall quality of the minimization stages of the program can only be tested with a large sample of data points- and require the visualization programs like PHASE to be completed. Also the 1.5 sec CPU time per point (which means a 4000 point diagram

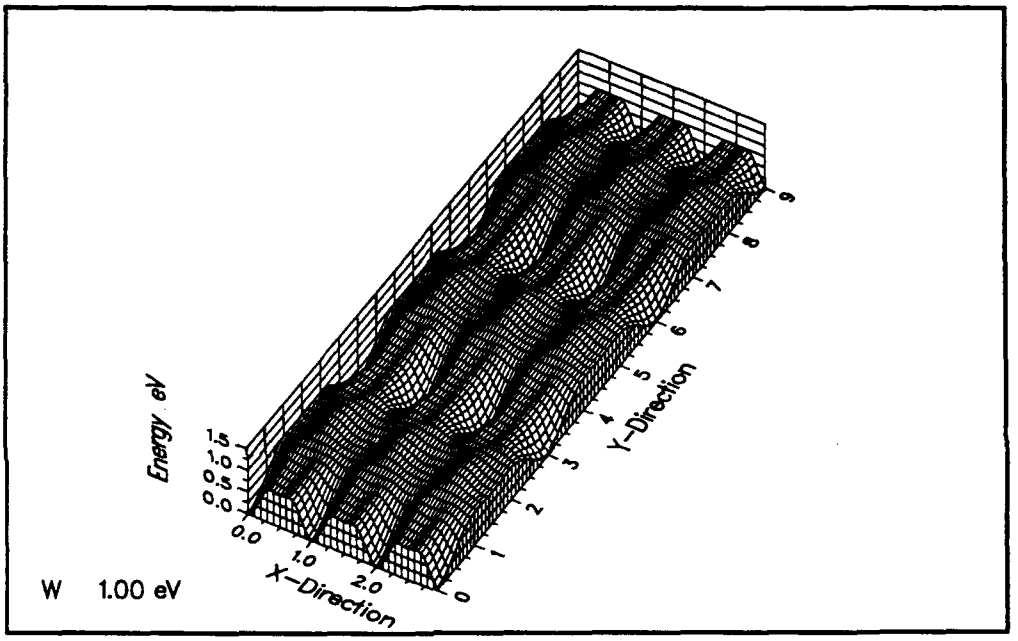

Figure 1. A representation of an adatom-substrate interaction potential which models the interaction between a diamond overgrowth and a BN {221} substrate, showing 3 × 3 unit cells.

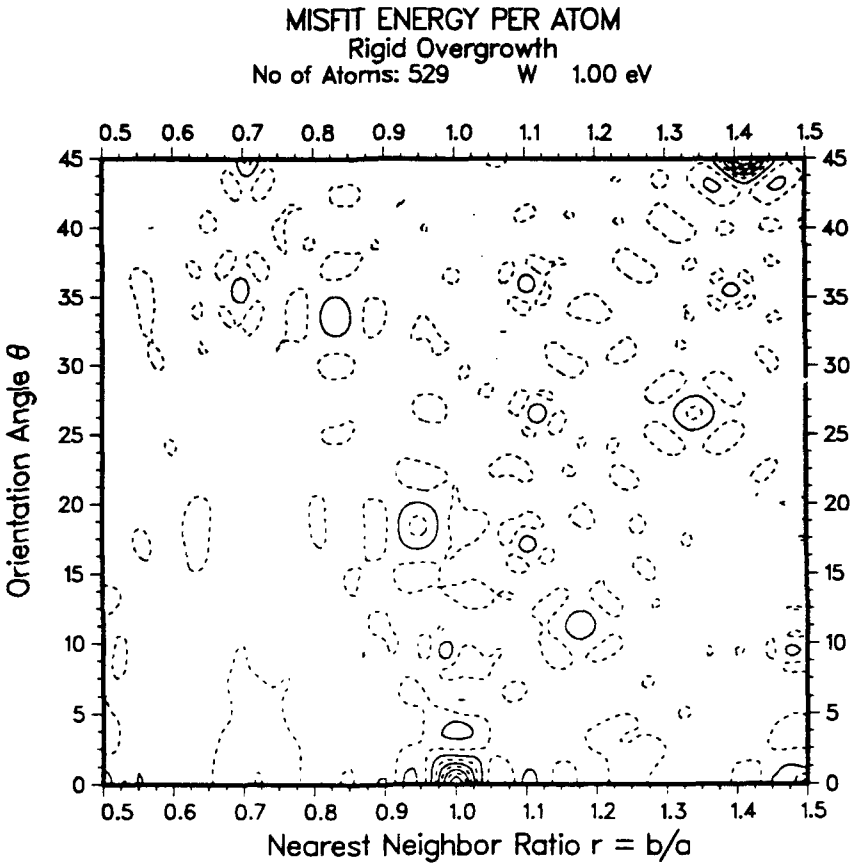

Figure 2. A contour representation of the misfit energy as a function of nearest neighbor ratio and orientation for a diamond structure in {100} on the BN {221} surface modelled in Fig. 1. Diamond and cubic boron nitride have a lattice parameter ratio of 0.9864.

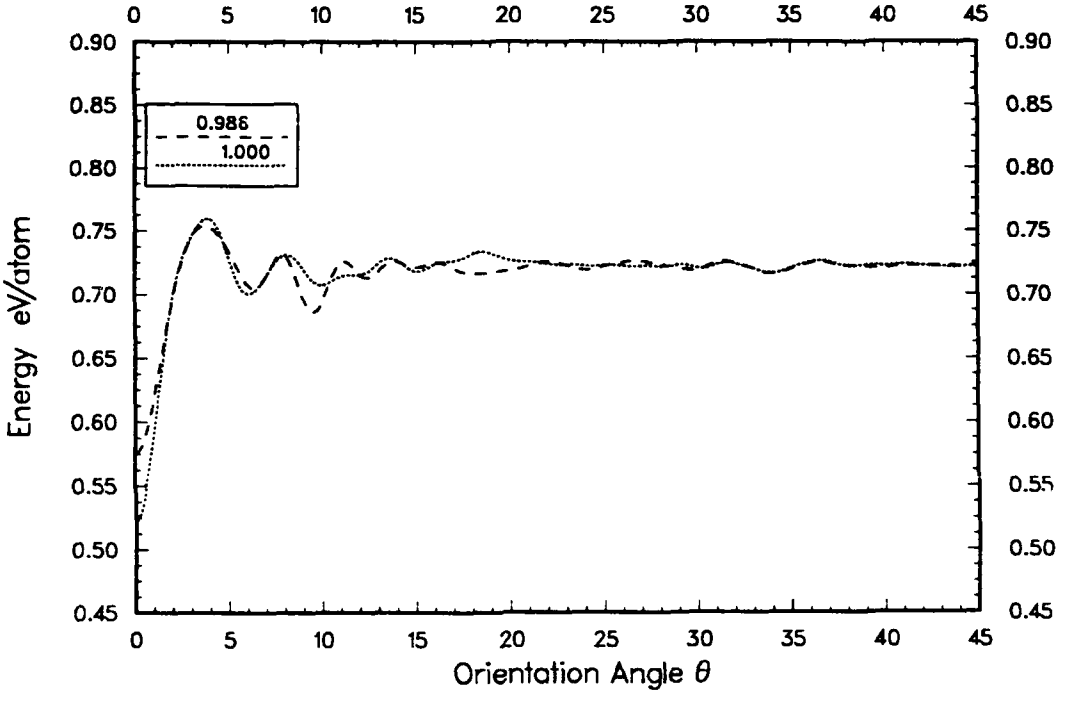

Figure 3. A cross sectional diagram of the misfit energy of the diamond {100} on cubic boron nitride {221} system for the nearest neighbor ratios 0.9864 and 1 (pseudomorphic case) showing the strong minimum in energy about θ=0°.

needs 100 minutes of CRAY -cpu time) must be reduced before these large scale tests can be run. Development of these visualization programs is under way, and once they are completed PSEUDO will be proved and optimized for both CPU performance and ease of use.

E. Conclusions

The suite of programs for the classical representation of a covalent structure grown on a covalent substrate material is nearing completion. The programs ELCON, (which transforms elastic constants for input to both ORPHEUS and PSEUDO) and MULTIMIS which applies a generalized form of the van der Merwe-Reiss rigid model suitable for the special requirements of these interfaces, are essentially complete.

The program PSEUDO, which provides data for determining thickness, orientational and structural lattice ratio transitions between epitaxial orientations by minimizing strain and misfit energies together, is in testing and polishing stages. The program which analyses and displays the output from PSEUDO, namely PHASE, exists only in rudimentary form, and needs to be generalized. Full optimization and testing of PSEUDO will be resumed once that program is complete.

Both MULTIMIS and PSEUDO need good estimates of the bonding strengths and the elastic constants in thin film structures. These will be generated from an Embedded Atom Method approach, a process which has begun. The skeletal molecular dynamics program has been completed, it dynamically simulates the movement of several tens of atoms which experience an embedded atom model potential derived by Dr. J. Beeler. In the next stages, this program will be adapted to use the Baskes, Nelson and Wright [12] Silicon and Germanium potentials formulated in the Modified Embedded Atom Method (bond directionality has been added to the pure method in this formulation). It is envisaged that these potentials can be used as prototypes for the development of the

alloyed covalent and metal covalent systems of interest to this project. Where necessary input data for the development of the specialized potentials can be provided from the density functional theory. (See for example the code DMOL [13], which is available on the CRAY.)

A future development seen for the PSEUDO program is an extension which will allow the substrate also to relax elastically. Clearly this simulation stage will only be of value once the behavioral parameters have been well characterized from the EAM models.

To summarize, immediate goals are (1) the completion of the PHASE analysis and visualization program, (2) the optimization of PSEUDO, (3) calculation of parameters for PSEUDO from the Embedded Atom Empirical and semi-empirical potentials and (4) the extension of PSEUDO to more than one elastic layer.

It is envisaged that goals 1 and 2 will be reached by the next reporting period, while (3) should be well under way. The development work for (4) should have begun by that time.

The long term goal of predicting band structures and resulting electro-optical properties will be addressed after these structural programs have been completed, but the density functional theoretical steps are early theoretical experiments in that direction.

III. AlN/GaN Superlattices Grown by Gas Source Molecular Beam Epitaxy

A. Introduction

Commercialization of light emitting optoelectronic devices in the previous decade stimulated considerable interest in those III-V nitrides which possess a direct energy gap in the UV region of the spectrum. A comprehensive review regarding the thin film and optoelectronic research in GaN prior to 1988 has recently been published [14].

Depositions of AlN and AlGaN have also been studied [15,16].

Bandgap engineering in the range of 3.4–6.2 eV can be achieved either by solid solutions or by superlattices of GaN and AlN. The latter are favored for several reasons. As has been shown for the GaAs/GaAlAs system [17,20], optoelectronic devices using multi–quantum well structures instead of heterostructures exhibit lower threshold current density, lower non–radiative recombination rate, narrower emission spectra and reduced sensitivity to temperature. The lattice parameter mismatch between AlN and GaN is only 2.5%, thus layered structures of these two materials offer a way of producing high quality, low dislocation density GaN– and/or AlN–based materials and devices. To our knowledge, superlattices of these two materials (or any other wurtzite semiconductor) have not been produced prior to this investigation. These are also the first semiconducting superlattices exhibiting band discontinuity well above 1 eV.

The following sections describe the procedures used to deposit and characterize the layered structures as well as detail the results and conclusions of this research.

B. Experimental Procedures

The growth system was a modified Perkin-Elmer 430 MBE system. Standard effusion cells were used for the evaporation of Ga and Al, while the nitrogen was activated in a small, MBE compatible, ECR plasma source [21].

The growth studies were conducted on (0001)-oriented a-SiC (6H polytype) and (0001) oriented epitaxial quality sapphire substrates, both of which have a hexagonal structure. All substrates were chemically cleaned and thermally desorbed in the vacuum at 900°C prior to the introduction in the growth chamber. All superlattices were grown under the same conditions, which are summarized in Table I.

TABLE I. Growth conditions

Nitrogen pressure	$1x10^{-4}$ Torr
Microwave power	50 W
Gallium temperature	990°C
Aluminum temperature	1120°C
Substrate temperature	400–750°C
Growth rate:	
GaN	≈2.5 nm/min
AlN	≈1.6 nm/min
GaN buffer layer thickness	140 nm
Period thickness	1.5–40 nm
Number of periods	20–200
Total growth time	6–7 hrs

Scanning Auger microprobe (SAM) (JEOL JAMP-30) analysis was used to determine the presence of impurities and the nominal compositions of the AlN and GaN layers. The superlattices were subsequently analyzed by x–ray diffractometry using $Cu_{K\beta}$ to determine layer period and the crystalline quality of the films. Transmission electron microscopy (TEM) (Hitachi H-800) and high resolution microscopy (HREM) (JEOL 200CX) were used for further analysis. Cross-sectional TEM specimens were prepared using standard techniques [22]. The luminescent properties of the samples grown on a(6H)-SiC were examined by cathodoluminescence. The spectra were taken at 77 K in the wavelength range of 200 to 800 nm using the excitation electron beam energies of 7 keV.

C. Experimental Results

1. Chemical Analysis

Figure 4 shows an Auger depth profile taken from a sample with 20 AlN/GaN double layers. The layers of each material were 10 nm thick. The profile indicates well defined layers. The spectra indicate nominal AlN and GaN compositions and some mixing of Ga and Al in the AlN and GaN layers, respectively. A small amount of interfacial mixing may be present; however, the Auger data exaggerate this phenomenon because of

insufficient depth resolution. This resolution in the sputter Auger technique depends on the escape depth of the Auger electrons (≈5 nm) and the depth resolution of the sputtering process (also ≈5 nm). For both reasons was the instrument's depth resolution in this study in the same range as the layer thickness. The fact that the Auger depth profiling exaggerates interlayer mixing for very thin layers can be proven by examination of the TEM results (see below) which show well defined layers even at a thickness of only two monolayers.

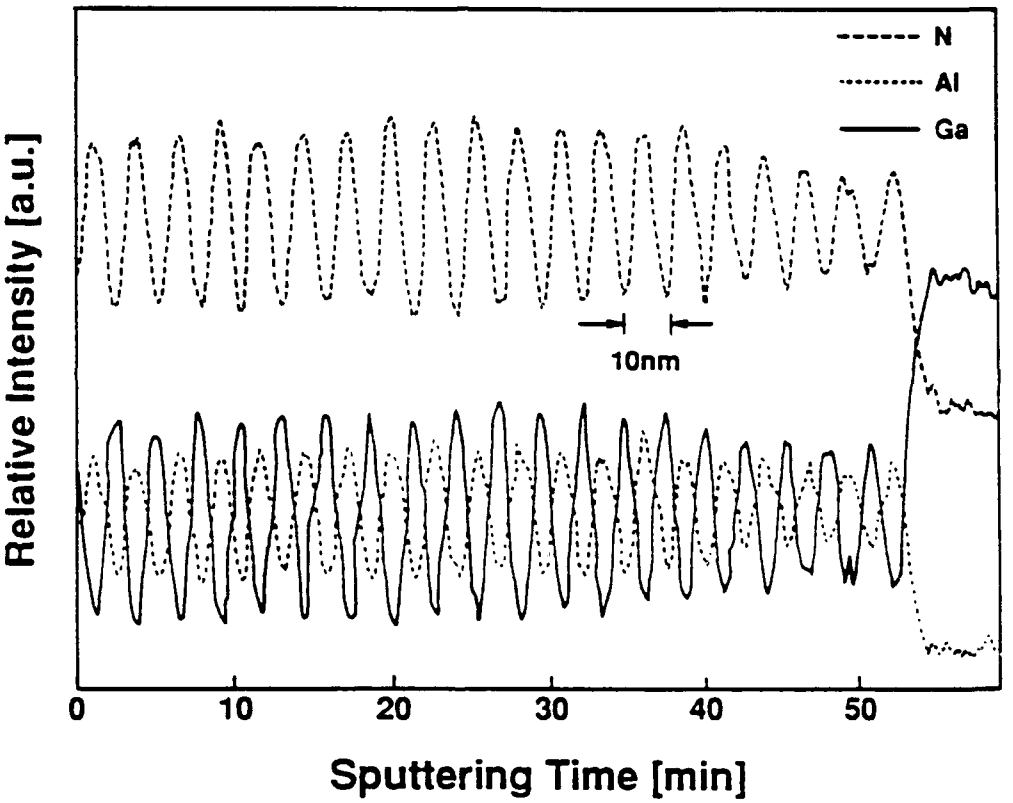

Figure 4. Auger depth profile taken from a sample with 20 AlN/GaN double layers. The layers of each material were 10 nm thick.

2. Structural and Microstructural Analyses

X-ray Analysis. Figures 5(a1–a3) show the evolution of the diffraction peaks as a function of decreasing AlN/GaN bilayer periodicity, P, which is given as:

$$P = t_{AlN} + t_{GaN} , \qquad (1)$$

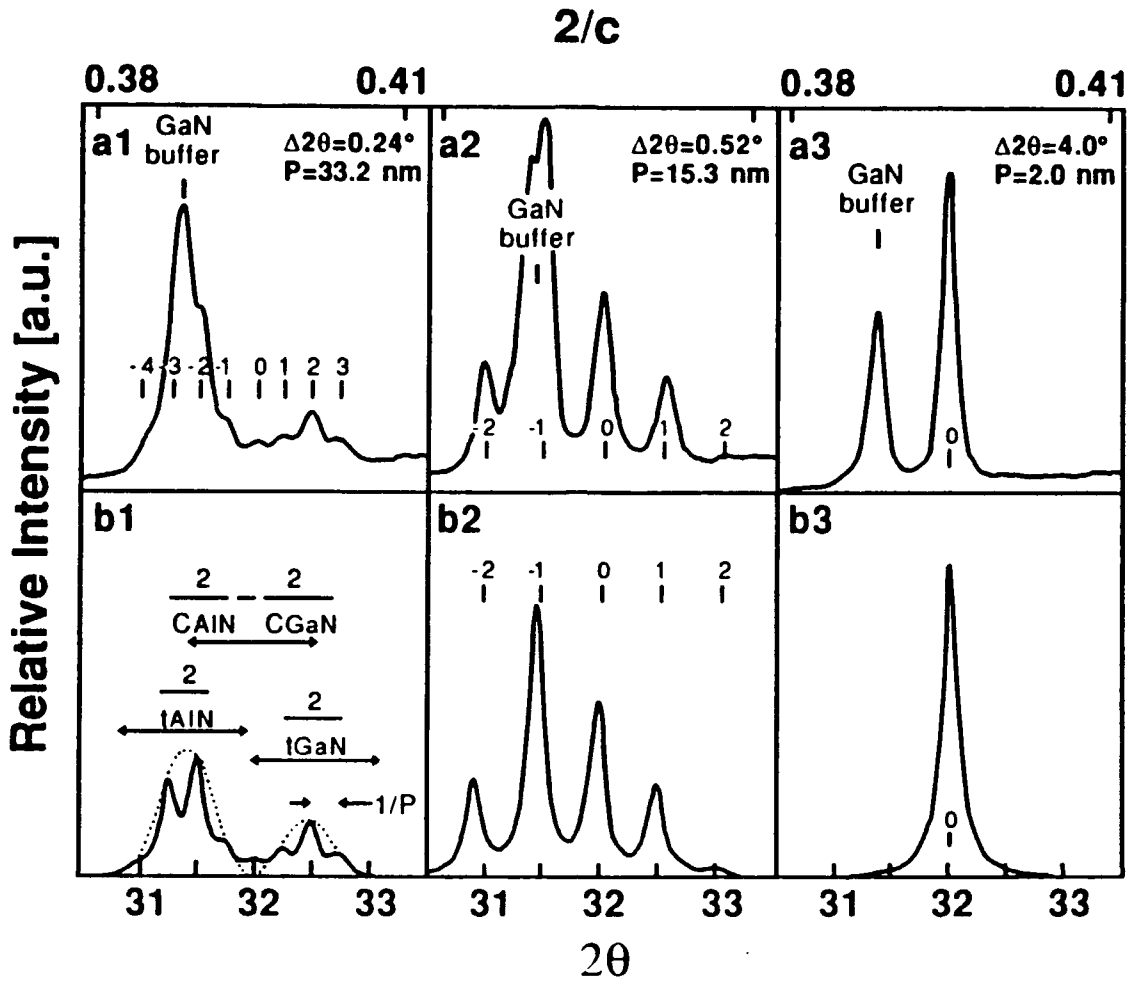

Figure 5. (a) X-ray diffraction spectra of the samples with different periodicities. Each pattern is characterized by the (0002) peak from the GaN buffer layer (marked by "GaN buffer") and a zero-order peak from AlN/GaN layers at $2\theta = 32°$ (marked by "0") with satellite peaks around it. An angular spacing, D2q, of satellite peaks and a calculated bilayer period, P, is given for each spectrum. (b) Diffraction spectra after the subtraction of the GaN buffer layer peak and the overall background. Figure (b1) illustrates the use of the spectra for the determination of different parameters (see text).

where t_{AlN} and t_{GaN} are the respective thicknesses of the individual layers of AlN and GaN. Each spectrum shows the (0002) diffraction peak from the GaN buffer layer, the zero order superlattice peak (marked "0") which represents the average vertical lattice parameter of the superlattice and the associated satellite peaks (marked from -4 to 3). The fact that the GaN and the zeroth–order superlattice peaks do not coincide shows that the superlattices are sufficiently thick to be structurally independent of the GaN buffer

layer. As such, the lattice constant in the structure is characteristic of the superlattice rather than the substrate. The biaxial strain is shared between the GaN and the AlN layers, as the GaN layers are biaxially compressed and the AlN layers are biaxially dilated.

Since the buffer layer peak is superimposed on the superlattice peaks, it makes the diffraction from the superlattice unclear. As such, each spectrum in Figures 5(a1-a3) was fitted with a sum of Lorentzian peaks followed by the subtraction of both the buffer layer peak and the overall background. This allows the evolution of the peaks with the change in superlattice period to be more easily observed. The resulting spectra are shown in Figures 5(b1–b3). In this latter set of spectra, the x–ray intensities are plotted as a function of 2/c, where c is the lattice parameter perpendicular to the superlattice. This is convenient for measuring the parameters P, t_{AlN}, t_{GaN}, c_{GaN}, and c_{AlN} directly from the spectra. A representative diffraction spectrum having marked parameters characteristic of a superlattice produced in this study is shown in Figure 5(b1).

Figure 5(b1) shows two almost completely separated sets of superlattice peaks, each of which represents one of the two materials. The center of the GaN envelope coincides with the GaN buffer layer peak. This indicates that both have the same vertical lattice spacings. Since the center of the AlN envelope also appears at the same angular position as one would expect for the (0002) peak of bulk AlN, this indicates that individual layers at this period have unchanged vertical lattice parameters and thus are relaxed with respect to each other.

As the period decreases, the positions of the envelopes change. This is believed to be related to the biaxial lattice distortion due to elastic strain. In Figure 5(b2) both sets of peaks begin to overlap, and the exact positions of the two envelopes become less obvious. As one moves toward even shorter periods the two envelopes can no longer be resolved. As a consequence of shorter periods the number of observable satellite peaks decreases. Figure 5(b3), which represents the diffraction spectrum of a superlattice with

P=2 nm, shows only the zero–order superlattice peak which is located approximately midway between the expected peaks for pure AlN and pure GaN. The peak corresponds to an interplanar spacing of 0.252 nm, which is intermediate between the spacings of the (0002) planes of AlN (0.249 nm) and GaN (0.258 nm) and represents the average spacing of the (0002) planes in the superlattice. Satellite peaks for this sample are out of the range of the scan, and are expected to be at ≈28° and ≈36°. As noted above, TEM results show a well defined layered structure; thus, there is no reason to believe that this peak arises from the homogeneous mixing of the two materials.

According to the diffraction results, the transition between the relaxed and strained structures occurs at a layer thickness between 6 and 8 nm. This is in good agreement with the calculated value of 7.5 nm as the critical thickness using the method of Matthews and Blakeslee [23]. In order to more accurately determine the critical thickness, the reflections from the planes with mixed indices (for example $(10\bar{1}1)$) should be studied.

Transmission Electron Microscopy. The periodicities calculated from the x-ray spectra were confirmed by the TEM images. Discrepancies between the two methods were found to be less than 5%.

Figure 6 shows a TEM image of 20 nm thick layers of AlN and GaN grown on (0001) a(6H)–SiC. GaN layers are dark and those of AlN are light. Layers are well defined and have few structural defects. The $(01\bar{1}0)$ diffraction pattern (inset), taken from the layered structure, confirms the monocrystalline nature of the film.

By contrast, structures grown on sapphire showed a columnar structure with slight misorientation. However, layers of the two materials within individual crystallites are well defined, and no misfit dislocations or other defects have been found for layers thinner than 7 nm. Even the structure containing 0.5 nm thick AlN layers (2 monolayers) and 1 nm thick GaN layers (4 monolayers), shown in Figure 7, show very good compositional contrast.

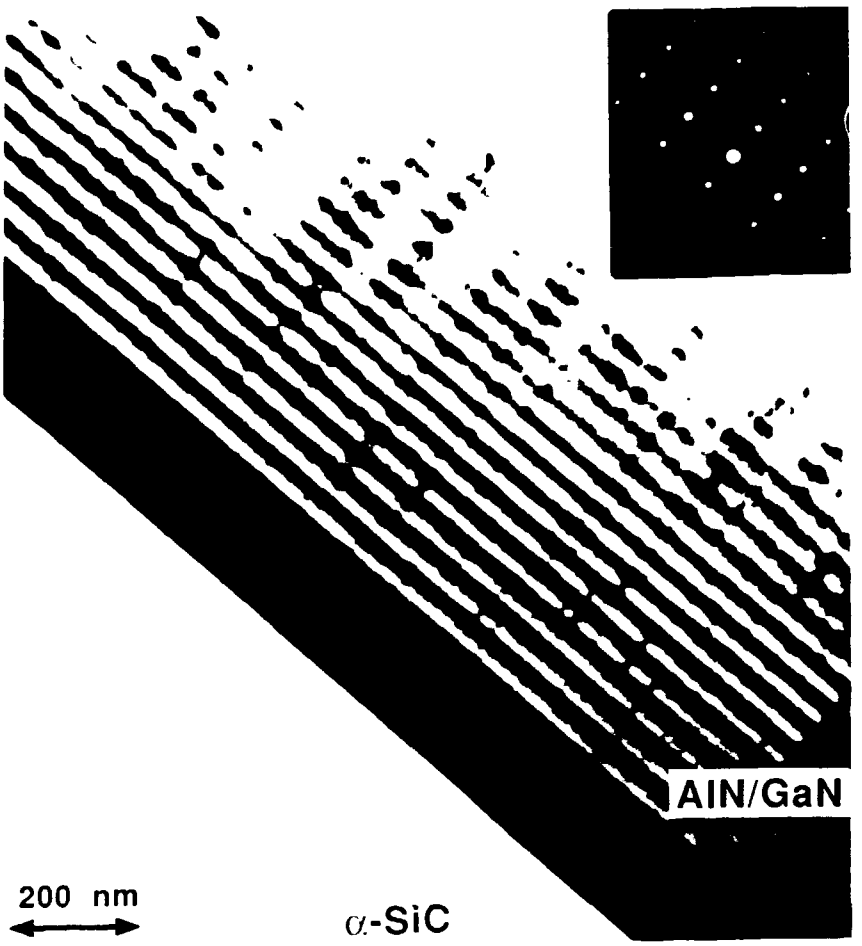

Figure 6. AlN/GaN superlattices grown on a(6H)-SiC. The thickness of the individual layers is 20 nm. Inset shows an electron diffraction pattern of this superlattice (zone axis $(01\bar{1}0)$), which confirms the crystalline quality.

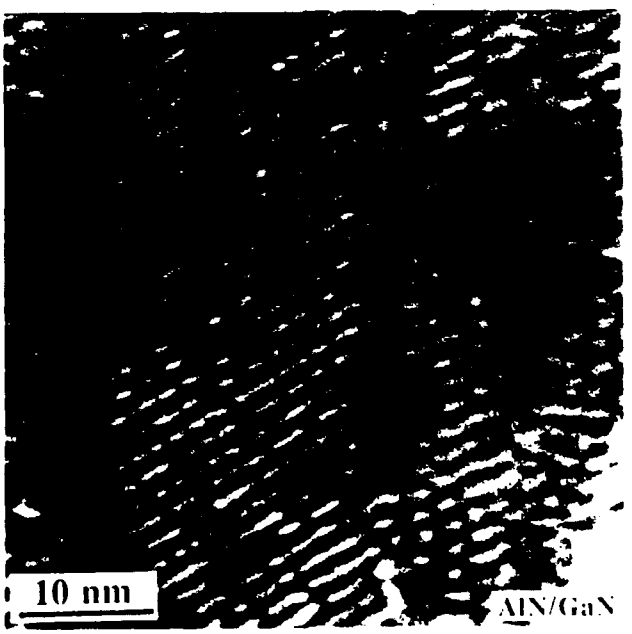

Figure 7: AlN/GaN superlattice grown on sapphire. The thickness of AlN and GaN layers is 0.5 nm and 1 nm, respectively.

3. Optical Characterization

The bandgap difference between AlN and GaN is 2.8 eV. Thus layers of these two materials produce almost one order of magnitude larger band discontinuities than are achieved in AlGaAs or InGaAs systems. As such, AlN/GaN superlattices may provide some interesting insights regarding the behavior of electrons and holes. For example, they have the potential of providing several well–separated confined electronic states.

Two different cases were examined: 1) the emission energy shift as a function of the layer thickness with the thicknesses of the GaN and AlN layers maintained equal (i. e. $t_{AlN} = t_{GaN} = \frac{P}{2}$) and 2) the emission energy shift as a function of the barrier (AlN) thickness, while the well (GaN) thickness was maintained constant at 1 nm.

The allowed energy bands for the electrons in the conduction band and for the holes in the valence band in the superlattice were calculated using a one-dimensional Krönig–Penney model [24]. According to this model an electron or a hole can occupy a particular energy state in the superlattice only if the following is true:

$$1 \geq \left|\cos\left[\frac{t_1(2mE)^{\frac{1}{2}}}{\hbar}\right]\cosh\left[\frac{t_2(2m(V-E))^{\frac{1}{2}}}{\hbar}\right] + \right.$$
$$\left. + \left(\frac{V}{E}-1\right)^{\frac{1}{2}}\left(\frac{V}{2E}-1\right)\sin\left[\frac{t_1(2mE)^{\frac{1}{2}}}{\hbar}\right]\sinh\left[\frac{t_2(2m(V-E))^{\frac{1}{2}}}{\hbar}\right]\right|$$

In this expression is E the energy of the electrons (holes), V the barrier height (band discontinuity), m the effective mass of the carriers, $\hbar$ is Planck's constant divided by 2p, and t_1 and t_2 are the well and barrier widths, respectively. Since there are no accepted values for the effective masses of the electrons and holes in either AlN or GaN, the average values of the available data were used [25]. The effective mass of the electrons was taken as $0.2m_o$ and that of the holes as $0.8m_o$.

A conduction and valence band discontinuity was determined by iteration to provide the best fit to the transition energies observed by cathodoluminescence. The best fit was obtained when one half of the total bandgap discontinuity (1.4 eV) was assigned

to the conduction band and one half to the valence band. The total bandgap discontinuity was calculated as the difference between the bandgaps of AlN and GaN. Because of the lack of data on the mechanical properties of semiconducting nitrides, the effect of the biaxial strain on the bandgap shift could not be included in the calculation, although it is expected to have a considerable influence on the bandgap of both materials.

The shaded areas in Figure 8(a) represent the lowest four calculated energy bands for the electrons in the conduction band and the holes in the valence band as a function of the individual layer thickness. The thicknesses of the AlN and GaN were considered equal in these calculations. The lowest transition energy in the superlattice at a particular layer thickness is obtained as the distance between the lower edge of the first energy band for the electrons and the upper edge of the first energy band for the holes. The arrows indicate the transitions in the structures with 1, 3, and 10 nm thick AlN and GaN layers. The different lengths of the arrows correspond to the emission energies observed by cathodoluminescence. The luminescence spectra for these three structures are shown in Figure 8(b). The spectra show sharp and well defined peaks with the energies above the bandgap of GaN. The width of the peaks increases with the layer thickness as the superlattice makes a transition from the pseudomorphic to a relaxed structure. The measured and calculated transition energies for these superlattices are collected in Table II.

The shaded areas in Figure 9(a) represent the lowest two calculated energy bands for the electrons and the lowest three energy bands for holes as a function of the barrier width at a constant well width of 1 nm. The arrows again indicate the measured transition energy of a particular structure. The measured luminescence spectra for 0.5 nm and 1 nm thick barriers are shown in Figure 9(b). The calculated and measured energies are summarized in Table III.

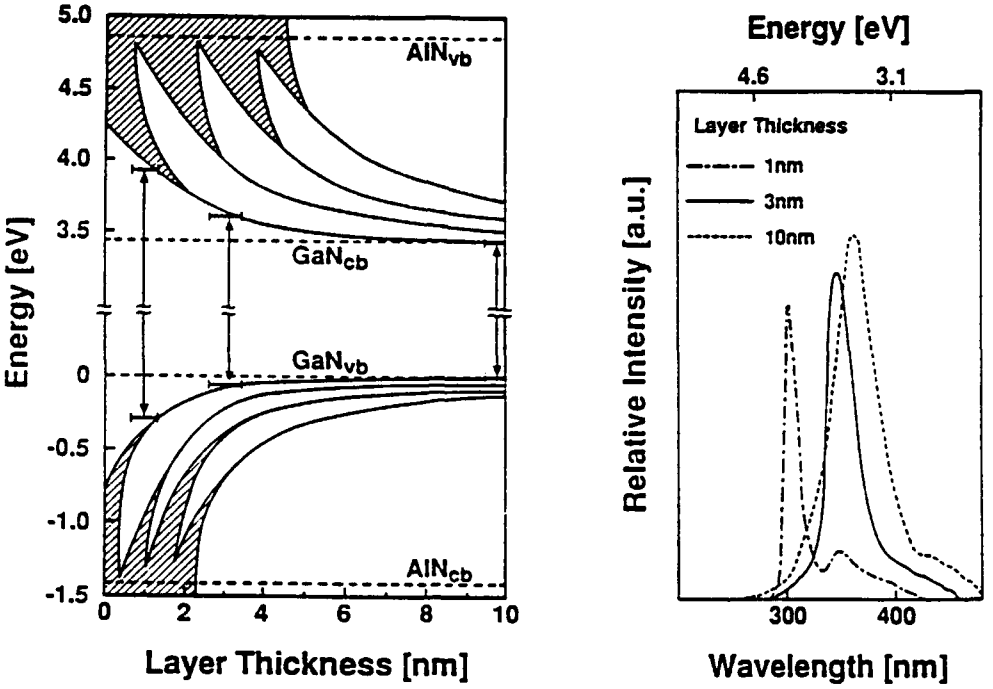

Figure 8: (a) The lowest four calculated energy bands for the electrons in the conduction band and the holes in the valence band as a function of the individual layer thickness while the thicknesses of the AlN and GaN were kept equal. The arrows indicate the transitions in the structures with 1, 3, and 10 nm thick layers, whose cathodoluminescence spectra shown in Figure 8(b).

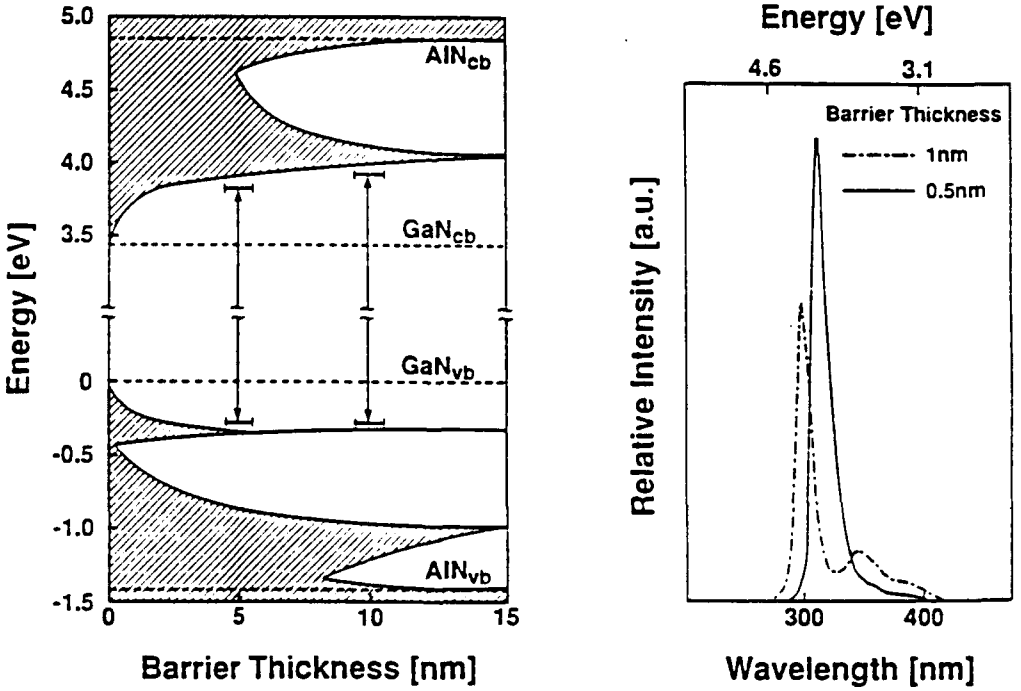

Figure 9: (a) The lowest two energy bands for the electrons and the lowest three energy bands for the holes as a function of the barrier width at a constant well width of 1 nm. The arrows indicate the measured transition energy of a particular structure. The measured luminescence spectra for 0.5 nm and 1 nm thick barriers are shown in Figure 9(b).

TABLE II. Calculated and measured transition energies for different layer thicknesses.

Layer thickness [nm]	$E_{calculated}$ [eV]	$E_{measured}$ [eV]	ΔE [meV]
1	4.29	4.11	180
3	3.64	3.47	170
10	3.42	3.42	≈0

TABLE III. Calculated and measured transition energies for different barrier thicknesses.

Layer thickness [nm]	$E_{calculated}$ [eV]	$E_{measured}$ [eV]	ΔE [meV]
0.5	4.19	3.93	260
1.0	4.29	4.11	180

An examination of both tables reveals the following information: 1) The highest transition energy shift observed in this study was above 700 meV and occurred in the superlattice with 1 nm thick barriers and wells. 2) The emission energy shift for the superlattice with 0.5 nm thick barriers was slightly lower than the previous value because of better coupling between adjacent wells (higher tunneling probability due to thinner barriers). 3) There exists an energy offset between the calculated and measured values, which was in the range of experimental error for 10 nm thick layers and increased to 170 meV for thinner layers and even up to 260 meV for superlattices with the thinnest barriers.

The reasons for the observed offset can be several. 1) There exists a possibility that the values for the effective masses used in the calculation are not accurate. For

example if the effective masses were larger, one would obtain lower theoretical values for the transition energies and, as such, a lower offset as well. 2) The lattice mismatch between AlN and GaN produces strain, which induces bandgap shift in both materials. This shift is expected to be rather high for the materials with 2% misfit (i.e., in the range of ≈100 meV) [26]. 3) Interfacial mixing of Al in GaN and Ga in AlN in the monolayer scale could significantly change the transition energy in superlattices having individual layers only a few monolayers thick.

The offset for the moderately thin layers (1 and 3 nm) seems to be fairly constant (180 and 170 meV), which would not be the case if only an error in the effective masses were in question. The fact, that the offset is negligible for thick layers (layers above the critical thickness, which are relaxed with respect to each other) and almost constant for the layers below the critical thickness (which are biaxially strained) implies a connection between the strain induced bandgap shift and the observed offset. As such, the luminescence data could be a rough indicator of whether a layered structure is pseudomorphic or not.

The offset for the superlattices with two monolayer thick barriers is even larger than that of the superlattices with moderately thin individual layers by an additional 90 meV. This jump, which could not be induced by the strain, is most likely the consequence of interfacial mixing, which lowers the barrier height and, as a consequence, causes a decrease in the transition energy. A more sophisticated model, which would include bandgap shift due to elastic strain and also assume one monolayer of interfacial mixing is expected to give much better agreement between the experimental data and theory.

D. Summary

Growth and characterization studies of AlN/GaN layered structures have been conducted using a modified gas source MBE technique. Layers as thin as two monolayers have been grown. X-ray and TEM results revealed strained material (no misfit

dislocations at the interfaces) for layers thinner than 6 nm and a completely relaxed structure for layers thicker than 10 nm. Cathodoluminescence studies showed a transition energy shift as high as 700 meV due to the quantum size effect. There exists a constant offset of 170 meV between the experimental and calculated values. Since this offset is present only for the pseudomorphic structures, it has been related to the strain induced bandgap shift of the two materials.

E. Future Research

The research on the growth of AlN, GaN and their layered structures in the MBE system. The primary goals are the improvement of the quality of materials, and the growth of p-type GaN and AlN. Mg will be used as the dopant for both compounds. Having achieved the quality and desired electrical properties, all efforts will be focused toward the growth of structures for simple optoelectronic devices.

In addition, a cathodo- and photoluminescence system will be designed and constructed in order to provide answers regarding the bandgaps and band energy shifts of compounds and superlattices. The system will be capable of measuring photon energies to 7 eV.

IV. Growth of SiC/AlN/GaN Pseudomorphic Structures

A. Introduction

A system designed for low temperature growth of monocrystalline SiC films and III-V nitrides by gas-source molecular beam epitaxy/atomic layer epitaxy (MBE/ALE) is virtually completed. Gaseous species will be provided to the sample surface using a pressure-controlled flow system which enables rapid switching of sources. Growth parameters can be controlled down to the monolayer level and reproducibly obtained using this technique. This deposition system will be used for low temperature growth of monocrystalline SiC thin films, SiC/AlN solid solutions and SiC/AlN pseudomorphic structures.

B. Experimental Procedure

1. Growth System

A schematic of the system to be used for gas-source MBE is shown in Figure 10. Samples are first introduced into a small load lock chamber, the chamber evacuated, and the samples subsequently transferred to the heating stage in the growth chamber. The load lock is used in order to increase sample throughput, as well as to keep the main deposition chamber under vacuum while samples are exchanged. It is pumped by a Balzers TPU 060 turbomolecular pump backed by a Sargent-Welch rotary vane pump. The load lock is operational, and pressures of 1×10^{-6} torr or below are easily reached in 30 minutes, at which point samples are transferred to the growth chamber.

The growth chamber will be utilized for both sample cleaning and deposition. Substrates will be cleaned prior to deposition by using an Ar^+ plasma to produce H_2^+ radicals from H_2 introduced into the system downstream from the plasma. The Ar^+ plasma will be obtained using an electron cyclotron resonance (ECR) plasma source developed in our laboratory [21]. This source is now installed, and will be characterized in the near future. To date, no published work has been performed on plasma cleaning of α–SiC.

Samples will be heated using a heater specially designed for this system. Heat will be produced by resistive heating of a coiled tungsten filament within a SiC-coated graphite cylindrical heating cavity lined with molybdenum and tungsten heat shielding. A high-purity pyrolitic BN disk is used as an insulating plate for holding the W coil in place. The sample is shielded from line-of-sight interactions from all parts of the heater not coated with SiC to minimize sample contamination. The heater shall be capable of temperatures of over 1000°C. Samples will also be rotated during growth to ensure sample uniformity.

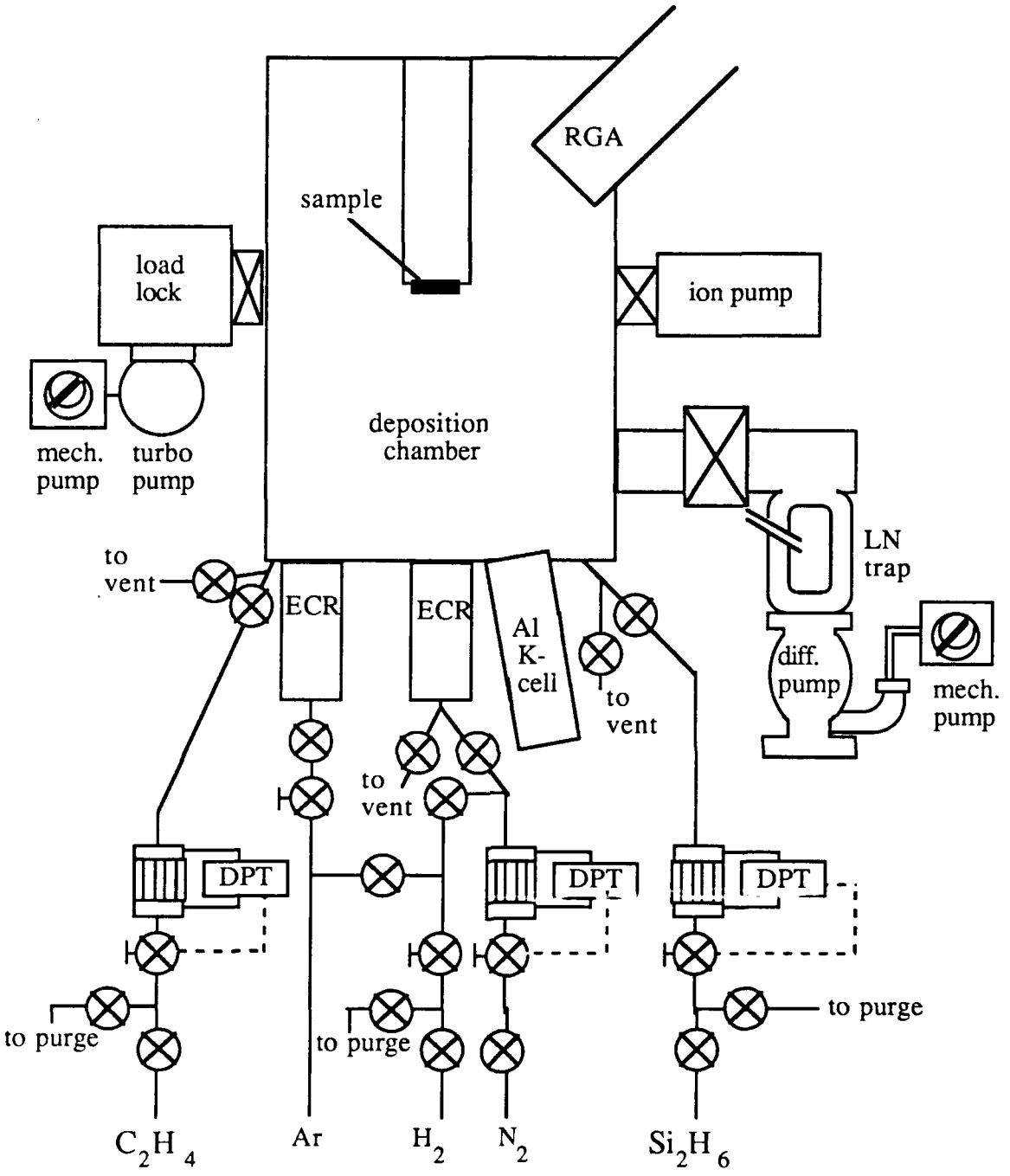

Figure 10. Schematic of Molecular Beam Epitaxy System

Species used in growth are introduced by way of the source flange. The source flange is equipped with ports for up to five solid sources and five gaseous sources. Disilane (Si_2H_6) will be used as a source of silicon, and will be supplied through a pressure-controlled flow system described in the next section. Ethylene (C_2H_4) will be

used as a source of carbon. It will be introduced through a specially designed ECR plasma source. This source will enable the introduction of ethylene downstream of an ECR-induced Ar^+ plasma. Aluminum will be provided by a solid-source MBE effusion cell made by EPI Systems. Diatomic nitrogen (N_2) decomposed with an ECR source will be used as a source of nitrogen. Mechanical air-actuated shutters will be used with all sources to aid rapid switching between sources for abrupt doping profiles.

In the case of MBE, the distance between collisions for each molecule is much longer than the dimensions of the deposition chamber. This implies that flow is in the molecular regime, and flow rates are too low for standard mass flow controllers. Gas mixtures can be used, but their use would compromise source purity and control. A method of flow measurement and control has been developed which works very well in the molecular regime [27]. It is based on the fact that in molecular flow, the conductance of a tube is not a function of pressure. The mass flow, Q, through an element can be expressed as

$$Q = C\Delta P$$

where ΔP is the pressure difference and C is the conductance. The conductance of a cylindrical tube or series of cylindrical tubes in molecular flow can be accurately calculated. If the pressure difference across this element of known conductance is measured, then the flow rate through this element can be easily found. The equipment used consists of a MKS CFE-0.5 precision molecular flow element, a MKS Model 120 differential capacitance manometer to measure the pressure difference across the element, and a Granville-Phillips Model 216 servo-driven leak valve and controller to control the gas flow to the element. The gas flow control system configuration is shown in Figure 11. Each gas used has its own flow control system. The entire flow control system, from the gas cabinet to the deposition chamber, will be exhausted for safety considerations. This type of system has been shown to enable the precise control of gas flow in the molecular regime, and can switch gases on in about 1 second and off in about 2 to 4 seconds [28].

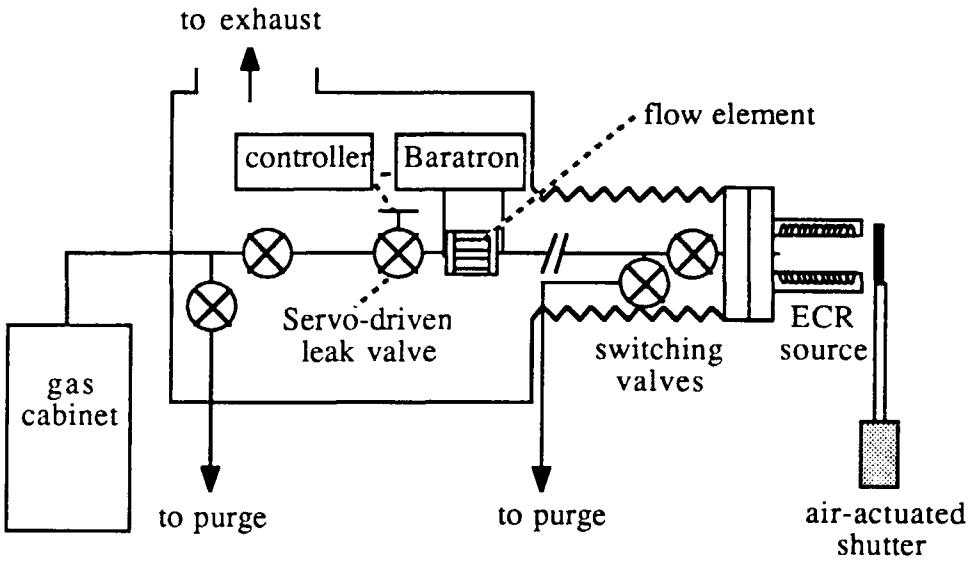

Figure 11. Valve System for Gaseous Sources

The chamber also contains a UTI-100C mass spectrometer, which will be used in order to determine species present during growth. Characterization of films using RHEED during growth is also planned. The system is pumped using a Varian VHS-6 2400 l/s diffusion pump with a Vacuum Generators UHV-quality liquid nitrogen cold trap backed by a rotary vane pump. A Perkin-Elmer ion pump has also been installed to help achieve UHV base pressures prior to deposition. Background pressures in the low 10^{-10} torr range are obtainable in this system.

2. Deposition Procedures

Growth of SiC films and AlN/SiC structures will take place on sublimation-grown, 1-inch diameter {0001} single-crystal 6H-SiC substrates provided by Cree Research. These samples shall by nature of the growth process and the subsequent cutting into wafer form, have some off-axis component. Immediately prior to introduction to the growth system, the oxide layer on each sample shall be removed by an HF acid solution. Samples will then be introduced into the growth chamber by way of the load lock. Samples will be cleaned *in situ* by the introduction of H_2 downstream from a ECR-induced remote Ar^+ plasma. Substrates will be heated to 473-673K for this cleaning step. Both

Ar and H_2 will be introduced in to the system by manual leak valves. Growth will be performed in the system described in the previous section.

Growth of SiC thin films will be performed using Si_2H_6 and C_2H_4 introduced as described in the previous section. Experimental flow rates of Si_2H_6 and C_2H_4 shall be in the 0.5-5 sccm range for SiC deposition. Empirical experiments will commence to find the proper growth temperature and flow rates of the SiC growth species. Growth temperatures to be used will be in the 1273-1673K range. Chemical vapor deposition (CVD) research conducted in our laboratory found an optimum growth temperature of 1773K [29,30], but growth species were not decomposed by other means prior to reaching the substrate. Doping experiments will begin once growth conditions for monocrystalline SiC growth have been optimized. Dopants to be used in this research are Al obtained from a standard MBE effusion cell and N obtained by decomposition of N_2 in an ECR plasma. Flow rates used will be from 10^{-3} to 1 sccm.

Once conditions for homoepitaxial growth of SiC have been optimized, growth of AlN/SiC pseudomorphic structures will begin. The same sources will be used for these experiments as for growth of SiC. Flow of Si_2H_6 and C_2H_4 will be switched on as flux from the Al MBE effusion cell and flow of N_2 into an Ar^+ ECR plasma are switched off, and vice versa. This will be done for various times depending on the thickness of layer desired. Flow of gaseous species will be switched using both the pressure-based flow system described previously and mechanical shutters. Flux of Al will be controlled by mechanical shuttering. N_2 into the Ar^+ plasma will be 1-5 sccm. In addition, experiments for the growth of AlN/SiC solid solutions will be performed. Flux of all species will be varied over a wide range. As information regarding possible precursors becomes available from a Si-SiC ALE system in our laboratory, growth of the films and structures using ALE will be performed.

Surface morphology of grown films will be examined using Nomarski optical microscopy and scanning electron microscopy. On those films with the best surface

morphology, samples for XTEM and plan-view TEM will be prepared. TEM with electron diffraction will be used to examine films as well as interfaces between layers. This information will be of prime importance in determining mechanisms of nucleation and growth in the obtained structures. Stress and misfit between layers will also be examined. Rutherford back-scattering spectroscopy (RBS) will be used to determine strain between individual layers. In order to easily determine relative misfit between layers, double-crystal X-ray diffraction will be used. Secondary ion mass spectrometry (SIMS) will be used to determine atomic concentrations of dopants and trace impurities present in the grown material. Auger electron spectroscopy will be used to obtain information regarding chemistry of individual layers and interfaces between layers.

C. Discussion

The primary hindrance to growth of AlN/SiC layers is the large disparity in growth temperature between AlN and SiC. It will be necessary for layers of the two materials to be deposited at the same temperature epitaxially. Homoepitaxial SiC growth by CVD in our laboratory occurs at a temperature of 1773K [29,30]. Monocrystalline growth of AlN generally occurs at 1173-1473K. This large temperature difference emphasizes the need to obtain low-temperature growth species for SiC to make growth of AlN/SiC layers feasible.

The primary obstacle to low-temperature growth of SiC is the difficulty in locating a suitable source for monomolecular carbon. Several methods for the deposition of solid carbon have been considered. The most promising of these is resistive heating of a graphite filament [31]. If the filament is heated to around 2500°C, a significant flux of carbon leaves the sample due to thermal evaporation. The majority of C leaving the filament has been shown to be monomolecular in nature. This method has been utilized for carbon doping of GaAs in an MBE system. Huge amounts of power and a filament with very large cross-section would be necessary in order to obtain a flux sufficient for MBE growth of a binary carbide such as SiC. This fact precludes the use of this method

at this time in this project. Other potential methods for solid-source deposition of C, such as laser evaporation and electron-beam evaporation, do not as yet yield large percentages of monomolecular carbon.

Gaseous sources of carbon such as hydrocarbons are relatively difficult to decompose. The growth temperature of SiC can be substantially lowered if the energy required for this decomposition can be decreased. One method which is useful in some instances is laser decomposition. High-energy monochromatic light, such as that produced by a laser, can impart sufficient energy to gaseous molecules to decompose them. Laser-enhanced chemical vapor deposition is a well-known technique for obtaining lower-temperature growth of many materials at pressures near one atmosphere. However, the efficiency of the decomposition process in the pressure range used in this research is extremely low.

Plasma decomposition is a proven method for low-temperature decomposition of gaseous species. The feasibility of an ECR source for monocrystalline growth of various materials in an MBE environment has been demonstrated [32, 33]. Decomposition of ethylene will utilize a previously mentioned NCSU-developed ECR source modified to allow the downstream introduction of a gaseous species. Downstream introduction of a carbon-containing species is necessary because of the electrically conducting nature of carbon deposits on the inside of the microwave cavity. Argon gas will be used to sustain the plasma. Valving will be placed as close to the source as possible to minimize dead space and enable the rapid switching on and off of the ethylene supply.

In addition to SiC films, SiC/AlN pseudomorphic layers and solid solutions will also be grown as a part of this research. Al and N will also be used as the primary dopants in SiC. Suitable sources of Al and N are thus required for this research. Nitrogen will be obtained by ECR plasma decomposition of N_2. MBE deposition of Al is possible either by thermal decomposition of an organometallic source, or thermal

evaporation of solid Al using an effusion cell. Both types of sources are commonly used in molecular beam epitaxy.

However, thermal decomposition of triethylalumimum (TEAl) and trimethylaluminum (TMAl) at temperatures above 600°C has long been known to result in significant carbon concentrations in GaAs films [34]. A relatively unknown organometallic source, triisobutyl- aluminum (TIBAl) has been shown to result in much lower carbon concentrations in Al films relative to other alkyls [35]. However, carbon concentrations on the order of 0.1 percent in GaAs grown by gas-source MBE still result from temperatures in the 700°C range using TIBAl. This is undoubtedly too high for electrical applications of AlN. As a result, a solid-source effusion cell will be used for Al deposition.

D. Conclusions and Future Research

A system for growth of monocrystalline SiC thin films and SiC/AlN solid solutions and pseudomorphic structures using gas-source MBE/ALE has been designed and is virtually completed. This system consists of a loading chamber and a deposition/cleaning chamber. The deposition chamber has the capability of using both solid and gaseous sources, and both will be used in this research. Gas flow will be controlled using a flow system based on measurement of the pressure drop across an element of constant conductance.

Samples will be cleaned prior to deposition using H^+ introduced downstream of an Ar^+ electron cyclotron resonance-induced plasma. Growth of SiC films and SiC/AlN structures will occur on 6H-SiC substrates provided by Cree Research, Inc. Silicon will be provided by thermal decomposition of disilane. Ethylene will be decomposed to an activated carbon-containing species using an electron cyclotron resonance plasma. Nitrogen will be decomposed using an ECR plasma. An MBE effusion cell will be used as a solid source for aluminum. Growth experiments on SiC will be performed to optimize growth parameters. *In situ* doping experiments will be performed. Growth of AlN/SiC

pseudomorphic layers and solid solutions will be performed. Once ALE growth precursors are found and tested on another system in our laboratory, these structures will be grown using ALE. Samples grown will be characterized using optical microscopy, SEM, TEM, RBS, X-ray diffraction, SIMS, and Auger.

V. References

1. van der Merwe, J. H., Phil Mag **45**, (1982) 127, 145, 159.
2. Reiss, H.; J Appl Phys **39**, (1968) 5045.
3. Braun, M. W. H., "Epitaxy on substrates with hexagonal lattice symmetry" DSc Thesis, University of Pretoria Nov 1987.
4. Bauer, E.; Z Kristallogr, **110**, (1958), 372.
5. van der Merwe, J. H. and E. Bauer, Phys Rev B, **39**, (1989), 3632.
6. van der Merwe, J. H. and M. W. H. Braun, "Interfaces, Lattices and Thin Films, Boston 1986," ed. J.D. Dow and I.K. Schuller, MRS Proceedings, **77**, (1987), 133.
7. Braun, M. W. H., H. S. Kong, J. T. Glass and R. F. Davis, "The Role of Geometric Considerations in the Diamond-Cubic Boron Nitride Heteroepitaxial System," Submitted to: J Appl Phys. (1990).
8. Frank, F. C. and J. H. van der Merwe, Proc Roy Soc, **A 198**, (1949) 205, 216; **A 200**, (1950) , 125, 261.
9. van der Mewe, J. H., Thin Solid Films, **74**, (1980), 129.
10. CA-DISSPLA, Computer Associates.
11. IMSL, International Mathematical and Statistical Library, Houston.
12. Baskes, M. I., J. S. Nelson, and A. F. Wright, Phys. Rev. B, **40**, (1989), 6085.
13. DMOL, Biosym Technologies Inc.
14. J. A. Edmond, J. Ryu, J. T. Glass, and C. H. Carter, Jr., Mat. Sci. & Eng. B **1**, 77 (1988).
15. P. M. Dryburgh, J. Cr. Growth **94**, 23 (1989).
16. Y. Koide, H. Itoh, M. R. H. Khan, K. Hiramatu, N. Sawaki, and I. Akasaki, J. Appl. Phys. **61**, 4540 (1987).
17. W. T. Tsang, Appl. Phys. Lett. **39**, 786 (1981).

18. M. G. Burt, Electron. Lett. **19**, 210 (1983).

19. P. Davson, G. Duggan, H. I. Ralph, and K. Woodbridge, Superlattices and Microstr. **1**, 173 (1985).

20. N. Holonyak, Jr., R. M. Kolbas, R. D. Dupuis, and P. D. Dapkus, IEEE J. Quantum Electron. QE **16**, 170 (1980).

21. Z. Sitar, M. J. Paisley, D. K. Smith, and R. F. Davis, Rev. Sci. Instr. **61**, 2407 (1990).

22. J. C. Bravman and R. Sinclair, J. Electron Microsc. Tech. **1**, 53 (1987).

23. J. W. Matthews and A. E. Blakeslee, J. Cryst. Growth **27**, 118 (1974).

24. For example; R. L. Liboff, *Introductory Quantum Mechanics*, Holden–Day, Inc., San Francisco (1980).

25. *Landoldt-Börnstein New Series*, Vol. III/17d, Springer–Verlag Berlin, Heidelberg, New York, Tokyo (1982).

26. N. G. Anderson, Ph. D. Thesis, North Carolina State Univesity, Dept. of El. and Comp. Eng. (1988).

27. R. A. Kiesling, J. J. Sullivan, and D. J. Santeler, J. Vac. Sci. Technol. **15**, 771 (1978).

28. H. Ishikawa, H. Ando, K. Kondo, A. Sandhu, E. Miyauchi, T. Fujii, and S. Hiyamizu, J. Vac. Sci. Technol. A **8**, 805 (1990).

29. H. S. Kong, H. J. Kim, J. A. Edmond, J. W. Palmour, J. Ryu, C. H. Carter, Jr., J. T. Glass, and R. F. Davis, Mat. Res. Soc. Symp. Proc. **97**, 233 (1987).

30. H. S. Kong, J. T. Glass, and R. F. Davis, J. Appl. Phys. **64**, 2672 (1988).

31. R. J. Malik, R. N. Nottenberg, E. F. Schubert, J. F. Walker, and R. W. Ryan, Appl. Phys. Lett. **53**, 2661 (1988).

32. Z. Sitar, M. J. Paisley, B. Yan, J. Ruan, W. J. Choyke, and R. F. Davis, J. Vac. Sci. Technol. B **8**, 316 (1990).

33. N. Yamamoto, N. Kondo, and Y. Nanishi, J. Cryst. Growth **96**, 705 (1989).

34. M. Weyers, N. Pütz, H. Heinecke, M. Heyen, H. Luth, and P. Balk, J. Electron. Mater. **15**, 57 (1986).

35. B. J. Lee, Y. M. Houng, and J. N. Miller, J. Cryst. Growth **105**, 168 (1990).